ACADEMIC PRESS

Available online at www.sciencedirect.com

SCIENCE DIRECT®

Journal of Solid State Chemistry 174 (2003) 69–73

JOURNAL OF SOLID STATE CHEMISTRY

http://elsevier.com/locate/jssc

Synthesis and red luminescence of Pr^{3+}-doped $CaTiO_3$ nanophosphor from polymer precursor

Yuexiao Pan,[a] Qiang Su,[a] Huifang Xu,[b] Tianhu Chen,[b] Weikun Ge,[c] Chunlei Yang,[c] and Mingmei Wu[a,b,*]

[a] *State Key Laboratory of Optoelectronic Materials and Technologies, School of Chemistry and Chemical Engineering, Sun Yat-Sen (Zhongshan) University, 135 Xingang Rd. W, Guangzhou 510275, People's Republic of China*

[b] *Department of Earth and Planetary Science, University of New Mexico, 200 Yale Blvd., Albuquerque, NM 87131, USA*

[c] *Department of Physics, Hong Kong University of Science and Technology, Clear Water Bay, Kowloon, Hong Kong, People's Republic of China*

Received 11 December 2002; received in revised form 14 March 2003; accepted 15 March 2003

Abstract

Uniform and sphere-like nanoparticles of crystalline Pr^{3+}-doped $CaTiO_3$ have been prepared from complex polymer precursor at 600°C, in which, metal atoms are previously dispersed by citric acid in ethylene glycol solvent. The decomposition process of the precursor, crystallization, and particle sizes of $CaTiO_3$ have been investigated by using thermal analysis, powder X-ray diffraction and transmission electron microscopy. Diffuse reflectance spectra, photoluminescence and decay curve indicate that a strong red emission located at the nearly NTCS "ideal red" site is deduced from the energy transfer from the band gap absorption to doping Pr^{3+} ions. The thermoluminescence curves exhibit that a potential long phosphorescent material based on Pr^{3+}-doped $CaTiO_3$ will be explored in future.

Keywords: Nanophosphor; $CaTiO_3$; Sol–gel chemistry; Red luminescence

1. Introduction

Recently, oxide phosphors have been found to be optimal candidate in field emission display (FED) and plasma display panel (PDP) devices as they are sufficiently conductive to release electric charges stored on the phosphor particle surfaces. Because oxides are resistant to high-density electron irradiation, the luminescent efficiency and thermal stability can be maintained under prolonged Coulomb loading. Much work has been concentrated on the novel phosphors based on Pr^{3+}-doped perovskite titanate [1–5], which are generally characterized with one strong and sharp emission peak at about 610 nm. In general, the doping of Pr^{3+} will increase the *n*-type conductivity of a titanate. Nanoparticles, on the other hand, have been recognized to hold tremendous potential in the area of photonic applications. Lanthanide-doped nanocrystalline oxides with particle diameters of 100 nm or less have been drawing particular interest recently [6]. Additionally, monodispersed, small and spherical particles are required for their application in FED [7] while coarse particles normally produce much more light scattering and increase the consumption of phosphors [8].

To obtain desired nanosized oxides and/or rare earth ions doped phosphors, wet chemistry such as coprecipitation [9], hydrothermal synthesis [10], colloidal chemistry [11–13] at relatively low temperature, has been used extensively, as starting materials in these methods can be mixed at molecular-level and the temperature for forming nanostructured products is relatively low. Citric acid can act as chelate ligands to metal ions to yield a rigid polyester network in which metal atoms are dispersed uniformly. Thus, the hydrolysis of the metal atoms can be inhibited and chemical processing can be controlled [14]. Using citric acid as a chelating agent has distinct advantages to preparing pure complex oxides of uniform nanoparticles at a relatively low temperature [2,15].

*Corresponding author. State Key Laboratory of Optoelectronic Materials and Technologies, School of Chemistry and Chemical Engineering, Sun Yat-Sen (Zhongshan) University, 135 Xingang Rd. W, Guangzhou 510275, People's Republic of China. Fax: +86-20-84111038.

E-mail address: ceswmm@zsu.edu.cn (M. Wu).

0022-4596/03/$ - see front matter © 2003 Elsevier Science (USA). All rights reserved.
doi:10.1016/S0022-4596(03)00175-0

$CaTiO_3$ is a chemically and thermally stable complex oxide, and has been widely used in electronic devices as a dielectric material. Pr^{3+}-doped $CaTiO_3$, as a relatively new luminescence material, exhibits red cathodluminescence located at $x = 0.680$ and $y = 0.311$ in the CIE coordinate [4]. The CIE coordinate is very close to that of the NTSC "ideal red" [3]. In addition, it is a potential red long persistent phosphor, which will probably substitute conventional sulfides in applications. New and excellent red long decay phosphors are becoming more and more important in science and technology, especially for white light, since blue and green long decay phosphors have been more developed than the red one. Up to the present, much work has been focused on this novel red phosphor, which has potential application in optoelectronic industry [4,5].

Besides lower temperature processing to prepare dispersed and uniform nanocrystalline particles, it is necessary to protect both Pr^{3+} from oxidation and Ti(IV) from reduction spontaneously during calcinations, which can be achieved by the combustion of organic components in air flow that provide atmosphere with suitable strength of reduction–oxidation. In this paper, we present the preparation and luminescence of ultrafine $CaTiO_3$:Pr, a red nanophosphor formed from a citric acid chelating precursor.

2. Experimental

2.1. Preparation

Pr_6O_{11} was dissolved in HNO_3 and an apple green $Pr(NO_3)_3$ solution was formed. Excess HNO_3 was removed by evaporation in fume cupboard. *n*-Titanium butoxide $Ti(OC_4H_9)_4$ was added to a mixed solvent of citric acid and ethylene glycol (EG) under a constantly magnetic stirring, until the solvent became transparent. $Ca(NO_3)_2$ solution was prepared by dissolving $CaCO_3$ in HNO_3 and excess HNO_3 was removed by evaporation in fume cupboard. The mixed solution of $Ca(NO_3)_2$ and $Pr(NO_3)_3$ with a molar ratio of 1000 CaO:2.0 PrO_2, was added dropwise to the above titanium organic solution slowly to avoid titanium butoxide hydrolyzing, until the molar ratio of calcium to titanium was up to unity. By heating at 200°C for 5 h, the solution color changed from pale yellow to bright yellow, and then brown. When the excess solvent was removed, the solution became more viscous but without any visible precipitation or turbidity. At last, dark-brown glassy resin-like substance was obtained. After further firing at 400°C for 2 h, a dry dark solid mass was obtained. After it was cooled to room temperature, it was ground slightly into powder with agate mortar. The black powder was called as precursor in this work. Ultrafine white powders were obtained after calcinations at a temperature of/or over 600°C for 5 h or a longer period in air.

2.2. Characterization

Thermogravimetric (TG) analysis of the precursor was carried out in air flow on a NETZSCH TG 209 TGA instrument from ambient temperature to 930°C with a heating rate of 10°C/min. Products were characterized by powder X-ray diffraction (XRD) collected on a Philips Model PW1830 diffractometer with a graphite monochromator and Cu$K\alpha$ radiation ($\lambda = 0.1541$ nm). Particle sizes and shapes were observed by transmission electron microscopy (TEM) on JEM-1010 electron microscope under an accelerated voltage of 100 kV. A sample for TEM examination was prepared by depositing an ultrasonically dispersed suspension of powder from a mixed solution of alcohol and water on a carbon-coated copper grid. Diffuse reflectance spectra were taken on a Cary 100 spectrophotometer. Photoluminescence spectra were recorded using a SPEX Fluorolog-2 spectrofluorometer, while long afterglow emissions were recorded on a photomultiplier of SPEX Fluorolog-Spectrofluorometer after irradiation by a UVP Standard mercury lamp peaking at 362 nm with a power density of 3300 lux for 10 min. For the measurement of decay time, the photoluminescence signal detected by the photomultiplier tube was analyzed on a sr400 photon counter. The xeon lamp dispersed by a spex1681 spectrometer was used as the excitation light source. The resolution of the system was about 5 ns. Thermoluminescence (TL) glow curves at a temperature range from 20°C to 500°C at a heating rate of 2°C/s were detected on FJ-427A TL-meter of Beijing Nuclear Instrument Factory. All measurements except TL spectra were carried out at room temperature.

3. Results and discussion

3.1. Synthesis of $CaTiO_3$ nanophosphor

The weight loss of the black precursor can be divided into three stages according to the TG-DTG curves as shown in Fig. 1. The weight loss up to 100°C is mainly attributed to the adsorbed moisture from air. The last two stages with major weight loss up to 600°C result from the decomposition and evaporation of complex network and organic molecules. Although the organic components can be decomposed completely only at 600°C, $CaTiO_3$ have crystallized at 500°C (Fig. 2a). As illustrated in Fig. 2, phase-pure and crystalline $CaTiO_3$ particles are prepared at 600°C, which are further characterized by TEM. Crystalline sizes calculated from full-width at half-maximum (FWHM) by using Scherrer's equation are around 10 nm, which is in

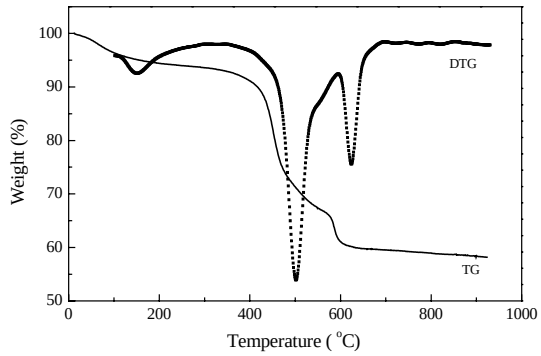

Fig. 1. Thermogravimeric (TG) curve (solid line) and differential thermogravimeric (DTG) curve (dotted line) of the polymeric precursor powder.

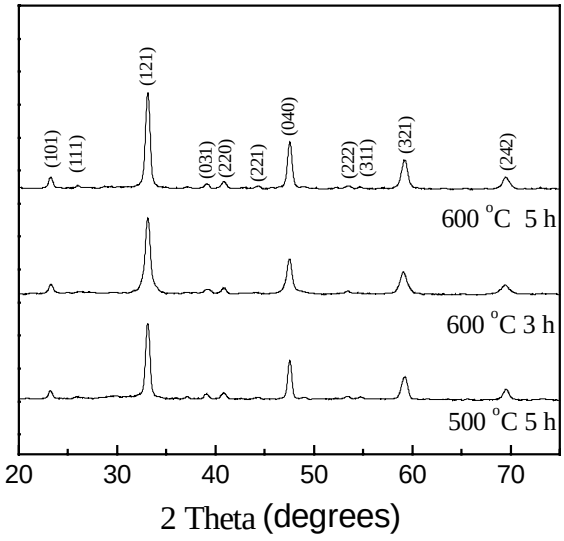

Fig. 2. Powder XRD patterns of $CaTiO_3$ obtained at 500°C for 5 h (a), 600°C for 3 h (b), and 600°C for 5 h (c).

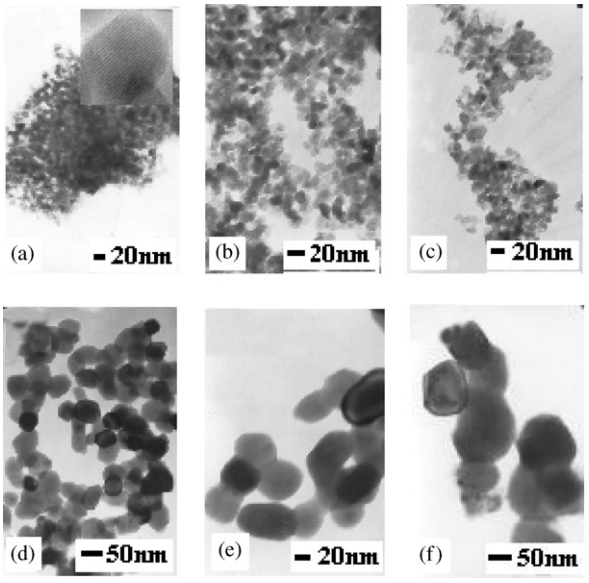

Fig. 3. TEM images of products prepared at 600°C for 3 h (a), 5 h (b) and 8 h (c); at 700°C (d), 800°C (e), and 900°C (f) for 5 h. The insert on the top-right of the photo (a) is a high-resolution TEM of a $CaTiO_3$ nanograin with clear lattice fringes indicating its good crystallinity.

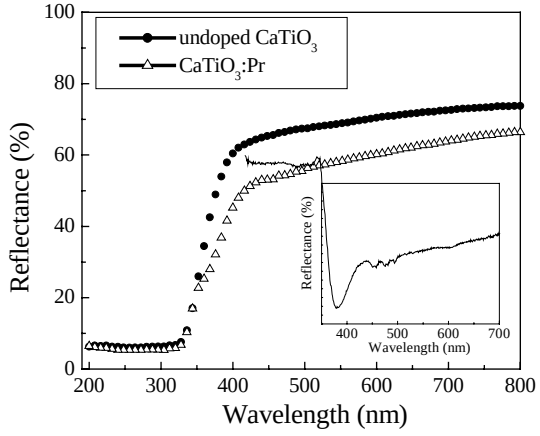

Fig. 4. Diffuse reflectance spectra of undoped and Pr^{3+}-doped $CaTiO_3$; Inset: enlarged difference of the two curves.

accordance with the results supplied by TEM observation (Fig. 3a). TEM photos in Fig. 3 indicate that much larger $CaTiO_3$ nanograins are produced at higher temperature. For example, $CaTiO_3$ particles of about 60 nm are obtained at 900°C for 5 h. At 600°C for 8 h, the particle size remains smaller than 15 nm, which is a higher reaction temperature significant for promoting the growth of $CaTiO_3$ particles (Fig. 3).

Here, phase-pure crystalline $CaTiO_3$ nanograins can be produced at 600°C, a much lower temperature than normal solid-state reaction to produce phase-pure $CaTiO_3$. This is because the citric acid can chelate metal atoms and these metal atoms disperse at molecular level, showing high activity as the bonds between metal atoms and ligands are broken. Moreover, due to the metal atoms separated by organic molecules being present in the network, uniform and dispersed nanocrystalline $CaTiO_3$ can be obtained through calcinations. Based on this concept, red nanophosphor of Pr^{3+}-doped $CaTiO_3$ is successfully prepared. The presence of Pr^{3+} in $CaTiO_3$ and its luminescent properties are further described as follows.

3.2. Luminescence

As shown in Fig. 4, the first derivative of the reflectance curve gives a peak at around 350 nm, which indicates the band gap of $CaTiO_3$ is around 3.55 eV. A trace doping of Pr^{3+} demonstrates a weak absorption shoulder maximum at about 390 nm, which is attributed to $4f-5d$ transitions of Pr^{3+} ions. Without doubt, the three weak absorption peaks in the range 450–500 nm are due to the transitions of Pr^{3+} from ground state to excited state ^3P_J ($J = 0, 1, 2$), while the weak peak at

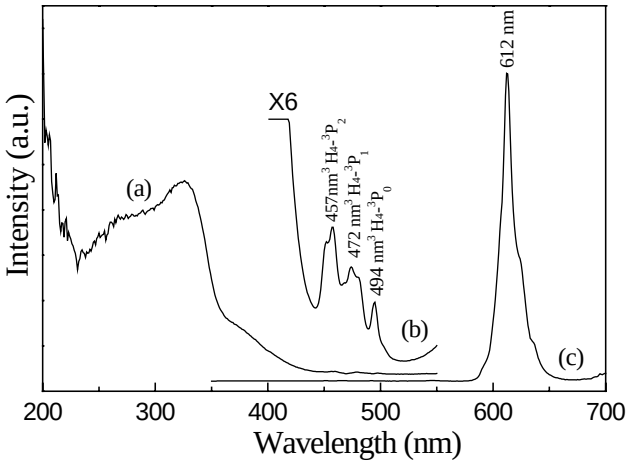

Fig. 5. Photoluminescence spectra of Pr^{3+}-doped $CaTiO_3$: excitation spectrum (a) and its enlarged one (b) ($\lambda_{em} = 612$ nm), and emission spectrum (c) ($\lambda_{ex} = 340$ nm).

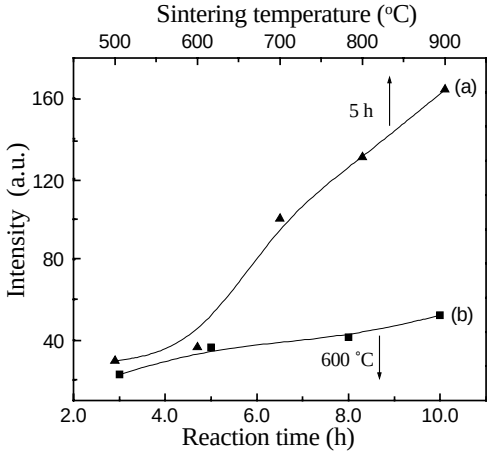

Fig. 6. Photoluminescence intensity varied with sintering temperature (a) and reaction time (b).

about 600 nm is assigned to the transition of Pr^{3+} from $^3H_4$ to $^1D_2$ (Fig. 4 inset).

Due to the band gap of $CaTiO_3$ host, a strong excitation band in the range of 250 and 350 nm is observed in Pr^{3+}-doped $CaTiO_3$ (Fig. 5a). These much weaker peaks at 457, 472 and 497 nm in the enlarged curve (Fig. 5b) are assigned to the transition of Pr^{3+} from $^3H_4$ to $^3P_2$, $^3P_1$ and $^3P_0$, respectively. Significantly, the typical $^1D_2$–$^3H_4$ transition of Pr^{3+} in $CaTiO_3$ host provides us strong and sharp emission at 612 nm. The unique red emission in the visible region from $CaTiO_3$ nanocrystals may offer us an opportunity to exploit novel PDP, FED and nanodevices.

The increasing intensity of nanocrystalline Pr^{3+}-doped $CaTiO_3$ with either reaction temperature or time in Fig. 6 implies that larger nanocrystallites can enhance the red emission. It has been reported that there is a critical nanocrystal size of Eu^{3+}-doped YVO_4 phosphor, at

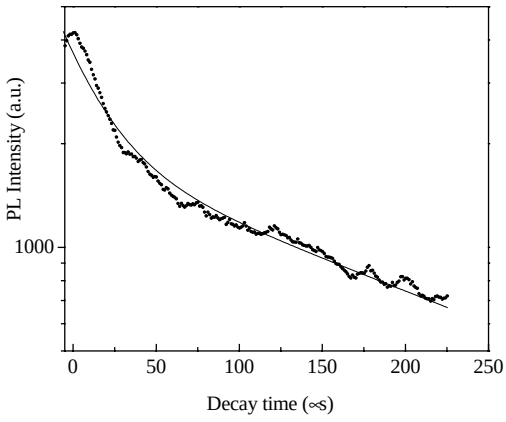

Fig. 7. Decay curve of the phosphorescence at 612 nm in $CaTiO_3$: Pr^{3+} ($\lambda_{em} = 362$ nm).

which the emission is the most intense [16]. However, it is difficult for us to prepare nearly white Pr^{3+}-doped $CaTiO_3$ powders with microsized grains while maintaining the control of valence states of both Pr and Ti at a much higher temperature than 900°C, especially for a longer reaction time. This is because Pr^{3+} will be readily oxidized to Pr^{4+} by sintering the sample in air at high temperature for a long time, whereas Ti^{4+} will be reduced to Ti^{3+} in reductive atmosphere and the powder will become gray. The suitable reductive atmosphere in our work is produced by combustion of citrate at temperatures lower than 1000°C.

The CIE coordinate ($x = 0.6897$, $y = 0.3013$), which is calculated from the emission spectra of our sample, is in good agreement with NTSC ideal red [3]. The decay of the emission $^3H_4$ to $^1D_2$ at 612 nm has two different speeds as shown in Fig. 7. The decay curve can be well fitted by double exponential equation: $I(t) = A\exp(-t/\tau_1) + B\exp(-t/\tau_2)$, where I is the luminescence intensity, A and B are constants, t is the time, τ_1 and τ_2 are the decay time for the exponential components, respectively. The τ_1 and τ_2 extracted from the fit are 24 and 230 μs, respectively. The rise time in the origin of the decay curve is attributed to the energy transfer.

In addition, long lasting phosphorescence is observed in our sample. In order to elucidate the doping of Pr^{3+} in $CaTiO_3$, TL glow curve of the phosphor above room temperature is supplied in Fig. 8. The lonely TL peak at around 70°C offers us a hint that the traps induced by Pr^{3+} ions are all the same in a suitable depth. That is a Pr^{3+} ion substitutes a Ca^{2+} ion to form a $[Pr^{\bullet}_{Ca}]$ defect, improving *n*-typed conductivity. The TL peak at around 70°C also shows probably long lasting phosphorescence. For measurement of long lasting property, a UVP standard mercury lamp peaking at 362 nm with a power density of 3300 lux is used to irradiate the products for 10 min and then the UVP is switched off. After 10 s, the

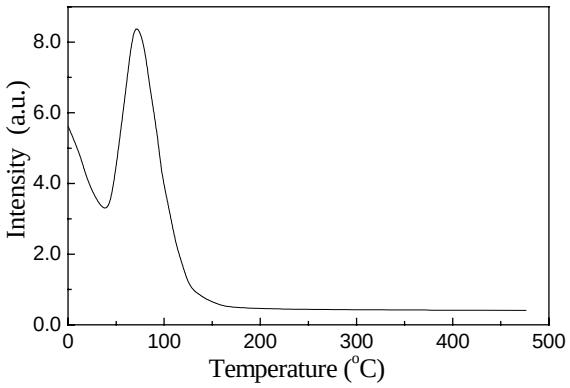

Fig. 8. TL glow curve of the phosphor excited by UVP light with energy flux of 0.6 mW/m^2 for 10 min.

intensity of the emission decreases to 0.04 cd/m^2 and it decreases to 0.01 cd/m^2 after 20 s. In addition, we can observe red long lasting phosphorescence in the sample with the naked eye after 20 s with the UVP standard mercury lamp switched off.

4. Conclusions

Nearly uniform sphere-like nanocrystalline phosphor $CaTiO_3$:Pr^{3+} has been prepared from a citric acidified polymer precursor. Both undoped and doped $CaTiO_3$ have strong absorptions in the UV region. The energy at excited state on the conducting level of nanophosphor can be efficiently transferred to the Pr^{3+} activators, leading to intense red emission. This will probably provide its potential applications in PDP, FED, and even in red nanolaser. The strong red emission from the Pr^{3+}-doped $CaTiO_3$ nanophosphor is located at a CIE coordinate ($x = 0.6897$, $y = 0.3013$), which approaches the NTSC ideal red color. The $CaTiO_3$:Pr^{3+} is also a potential red long lasting phosphor, indicating the possibility to substitute conventional sulfide in future optoelectronic devices.

Acknowledgments

This work was financially supported by the Provincial Natural Science foundation of Guangdong, NNSFC, and NSF of USA (NER02-10820 and CTS98-71292). We express our great appreciation to Dr. Chengyu Li in Changchun Institute of Applied Chemistry, Chinese Academy of Sciences.

References

[1] (a) Y.C. Kang, S.J. Choi, S.B. Park, S.H. Cho, J.S. Yoo, J.D. Lee, J. Aerosol Sci. 28 (1997) s541.
(b) S.H. Cho, J.S. Yoo, J.D. Lee, J. Electrochem. Soc. 143 (1996) L231.
(c) H. Yamamoto, S. Okamoto, Displays 21 (2000) 93.
(d) S. Okamoto, H. Kobayashi, J. Appl. Phys. 86 (1999) 5594.
[2] J.K. Park, H. Ryu, H.D. Park, S.Y. Choi, J. Eur. Ceram. Soc. 21 (2001) 535.
[3] S.S. Chadha, D.W. Smith, A. Vecht, C.S. Gibbons, 94 SID Digest 51 (1994) 1.
[4] (a) P.T. Diallo, P. Boutinaud, R. Mahiou, J. Caperaa, J.C. Cousseins, Phys. Stat. Sol. A 160 (1997) 255.
(b) S.M. Kim, J.I. Goo, T.O. Kim, J. Korean Ceram. Soc. 36 (1999) 1274.
[5] (a) P.T. Diallo, K. Jeanlouis, P. Bontinaud, R. Mahiou, J.C. Cousseins, J. Alloy. Compd. 323 (2001) 218.
(b) Y.C. Kang, D.J. Seo, S.B. Park, H.D. Park, Mater. Res. Bull. 37 (2002) 263.
(c) R.R. Martin, M. Shnya, T. Hiroto, U.S. Patent No. 5 650 094 (1997).
[6] (a) A. Patra, C.S. Friend, R. Kapoor, P.N. Prasad, J. Phys. Chem. B 106 (2002) 1909.
(b) J.A. Capobianco, F. Vetrone, J.C. Boyer, J. Phys. Chem. B 106 (2002) 1181.
(c) E. Zych, D. Hreniak, W. Strek, J. Phys. Chem. B 106 (2002) 3805.
[7] E.M. Vogel, N.C. Andreadakis, W.E. Quinn, T.J. Nelson, J. Am. Ceram. Soc. 21 (1987) 131.
[8] J.A. Castellano, Handbook of Display Technology, Vol. 19, Academic Press, San Diego, 1992.
[9] (a) C. Lind, A.P. Wilkinson, C.J. Rawn, E.A. Payzant, J. Mater. Chem. 11 (2001) 3354.
(b) M. Yashima, M. Kakihana, K. Ishii, Y. Ikuma, M. Yoshimura, J. Mater. Res. 11 (1996) 1410.
[10] (a) Y. Li, X. Duan, H. Liao, Y. Qian, Chem. Mater. 10 (1998) 17.
(b) H. Zhao, S. Feng, Chem. Mater. 11 (1999) 958.
(c) H. Meyssamy, K. Riwotzki, A. Kornowski, S. Naused, M. Haase, Adv. Mater. 11 (1999) 840.
(d) K. Riwotzki, M. Haase, J. Phys. Chem. B 102 (1998) 10129.
[11] G. Wakefield, E. Holland, P.J. Dobson, J.L. Hutchison, Adv. Mater. 13 (2001) 1557.
[12] A. Huignard, T. Gacoin, J.P. Boilot, Chem. Mater. 12 (2002) 1090.
[13] (a) M.M. Wu, J.B. Long, A.H. Huang, Y.J. Luo, S.H. Feng, R.R. Xu, Langmuir 15 (1999) 8822.
(b) M.M. Wu, G. Lin, D.H. Chen, G.G. Wang, D. He, S.H. Feng, R.R. Xu, Chem. Mater. 14 (2002) 1974.
(c) H.X. Zhang, C.H. Kam, Y. Zhou, X.Q. Han, S. Buddhudu, Y.L. Lam, Opt. Mater. 15 (2000) 47.
(d) Q. Li, L. Gao, D.S. Yan, Mater. Chem. Phys. 64 (2000) 41.
(e) I.C. Chen, T.M. Chen, J. Mater. Res. 16 (2001) 644.
[14] (a) W.S. Cho, E. Hamada, J. Alloy. Compd. 268 (1998) 78.
(b) W.S. Cho, E. Hamada, K. Takayanagi, J. Appl. Phys. 81 (1997) 3000.
[15] M. Kakihana, J. Sol–Gel Sci. Technol. 6 (1996) 7.
[16] K. Riwotzki, M. Haase, J. Phys. Chem. B 102 (1998) 10129.